NAIC-ID(RS)T-0704-94

NATIONAL AIR INTELLIGENCE CENTER

CHARACTERISTICS OF THERMAL LENS
IN A COPPER-VAPOR LASER

by

Hua Renzhong, Liang Peihui, et al.

HUMAN TRANSLATION

NAIC-ID(RS)T-0704-94 15 December 1994

MICROFICHE NR: 94C000564

CHARACTERISTICS OF THERMAL LENS IN A COPPER-VAPOR LASER

By: Hua Renzhong, Liang Peihui, et al.

English pages: 12

Source: Zhongguo Jiguang, Vol. A21, Nr. 3, March 1994; pp. 172-177

Country of origin: China
Translated by: Leo Kanner Associates
F33657-88-D-2188
Quality Control: Nancy L. Burns
Requester: NAIC/TATD/Bruce Armstrong
Approved for public release; Distribution unlimited.

GRAPHICS DISCLAIMER

All figures, graphics, tables, equations, etc. merged into this translation were extracted from the best quality copy available.

CHARACTERISTICS OF THERMAL LENS IN A COPPER-VAPOR LASER

Hua Renzhong, Liang Peihui, Ye Ren, Shen Qimin and Lei Jianqiu; all of Shanghai Institute of Optics and Fine Mechanics, Chinese Academy of Sciences, Shanghai 201800

Abstract The thermal lenses in operating copper vapor lasers and in the fused silica windows were measured by using of the deflection method and the interferometer method respectively. Experimental results show that the overall thermal lens is composed of a negative lens in the discharge gas and two postive lenses in two pieces of laser windows. Theoretical analysis agrees well with experimental results.

Key words copper vapor laser, thermal lens

I. Introduction

The thermal lens effect of a copper-vapor laser during its operation not only affects its light-beam quality, but also lowers the efficiency of the oscillation-gain system composed of multiple-unit equipment. Hence, one must carefully analyze the cause and regularities of the thermal lens effect. Zharikov et al determined that their equipment is based on a negative lens [1]; they analyzed gases in electrical discharge tube. However, Dixit, Bhatmagar and Amit et al determined, when adjusting the nonsteady-state cavity, that the cavity length should be shortened to collimate the output light beam [2-6]. This means that the copper-vapor laser operates like a positive lens. When the input electric power of the authors' copper-vapor laser was 4kW, it had the effect of a positive lens equivalent to about 100

meters [7]. To explain the difference between these two sets of experimental results, the authors noted that the fused silica window (in an electrical discharge tube with inhomogeneous radiation in the diametral direction) has the positive-lens effect induced by the temperature gradient. The authors' experimental results are explained on the basis of the composite gas-and-window lens model.

II. Analysis of Thermal Lens

As to the negative lens effect of electrical discharges in a gas and the positive lens effect of the window when the thermal lens of the laser is operating, in the following the analysis is made from a thermodynamic standpoint.

2.1. Negative lens effect of plasma electrically discharged gas during operation

The electrical discharge tube is symmetrically circular. From references [8, 9], the input power can be considered as uniformly distributed in the electrical discharge tube; the diametral-direction temperature distribution in the gas is

$$T(r) = \left[T_{wall}^{m+1} + \frac{P(m+1)}{4\lambda_0}(R^2 - r^2)\right]^{1/(m+1)} \tag{1}$$

In the equation, T_{wall} is the temperature at the tube wall; P is the input power density; λ is the coefficient of thermal conductivity of the gas; and R is radius of the electrical discharge tube. By taking m= 0.639, $\lambda_0 = 1.27 \times 10^{-3}$ (MKS)[9] the above-mentioned temperature distribution is in agreement with the experimental results in reference [10].

For a low-temperature electrically discharged gas, apply the analytical method as shown in reference [1]. The equation of state is

$$P = N(r)\, kT(r) \tag{2}$$

In the equation, P is the pressure intensity of a gas in the electrical discharge tube; k is Boltzmann's constant; N(r) is the gas density at a point that is at the distance r from the axial center.

The relation between the refractivity n(r) of the gas medium and N(r) can be expressed by the Gladston-Dale formula.

$$n(r) = 1 + C_{equ} N(r) \tag{3}$$

In the equation, C_{equ} is the equivalent G-D constant. In the copper-vapor laser device, C_{equ} is primarily determined by the Ne gas [1]. When the gas pressure of Ne increases, C_{equ} also increases somewhat.

Assume that the spacing between two windows of the laser device is l and that the temperature distribution deviates only slightly in the axial direction. Then from Eqs. 1, 2 and 3, by comparing the light rays at a point with r as the distance from the axial center, and with the light beam passing through the axial center after passing through the electrical discharge tube, the aberration is $\delta_{gas}(r)$

$$\delta_{gas}(r) = l[n(0) - n(r)] = -\frac{lC_{equ}\,p}{k}\left(\frac{1}{T(r)} - \frac{1}{T(0)}\right) \tag{4}$$

In the equation, T(0) is the temperature at the axial center

$$T(0) = \left(T_{wall}^{(m+1)} + \frac{P(m+1)}{4\lambda_0} R^2\right)^{1/(m+1)} \tag{5}$$

When r is relatively small compared to R $\quad \frac{P(m+1)\,r^2}{4\lambda_0 T(0)^{(m+1)}} \ll 1$

The following approximation can be made for $\delta_{gas}(r)$

$$\delta_{gas}(r) = -\frac{lC_{equ}\,p}{k}\left\{\frac{1}{T(0)\left[1 - \frac{P(m+1)\,r^2}{4\lambda_0 T(0)^{(m+1)}}\right]^{1/(m+1)}} - \frac{1}{T(0)}\right\} \simeq -\frac{lC_{equ}\,pP}{4\lambda_0 kT(0)^{(m+1)}} \times \frac{r^2}{T(r)} \tag{6}$$

2.2. Positive lens effect after absorbing radiation at window

There is very little absorption of the laser by the fused

silica window. At the window opening, the temperature distribution is determined by the heat conduction of the gas within the electrical discharge tube, by the radiation absorption in the electrical discharge tube at the window opening, and by the boundary conditions surrounding the window opening. When heat equilibrium is reached, the distribution of the temperature field is circularly symmetric. When a cylindrical coordinate system is used (r,z,φ), the origin is at the center of inner plane inside the window. The z-axis points outward from the axial center of the electrical discharge tube. The temperature distribution at the window opening can be approximately revealed with the polynomial

$$T(r,z) = T(0,z) + \sum_{n=1}^{\infty} a_n(z)\, r^{2n} \tag{7}$$

In the equation, T(0, z) is the highest temperature on a plane perpendicular to the axis center, and at the distance z from the origin. For the heat distribution in a low-temperature region at the fringe, $a_1(z) < 0, a_2(z), a_3(z)$ (and so on) determine the deviation between the actual temperature distribution, and the parabola-pattern distribution.

For a silica window, the approximation of thin specimen is satisfied when the thickness $d \leq 0.5D$ (D is the window radius). When the birefringence effects of the diametral- and tangential-direction stresses are approximately equal, aberration $\delta_{win}(r)$, after light rays pass through the window opening is [15]

$$\delta_{win}(r) = d\delta T(r)[dn/dT + (n-1)a(1+v) + n^3 aP'/2] \tag{8}$$

In the equation,

$$\delta T(r) = \frac{1}{d}\int_0^d [T(0,z) - T(r,z)]dz = \frac{1}{d}\sum_{n=1}^{\infty}\int_0^d [-a_n(z)]dz r^{2n} \tag{9}$$

$\delta T(r)$ is the difference between the mean temperature at the center of window opening and the mean temperature at a point whose distance from the center is r. dn/dT is the temperature coefficient of refractivity; a is the linear expansion coefficient; v is the Poisson ratio; and P' is the photoelastic coefficient. For a simplified expression, let

$$b_n = \int_0^d [-a_n(z)]dz \tag{10}$$

$$w_k = dn/dT + (n-1)\alpha(1+\nu) + n^3\alpha P'/2 \tag{11}$$

Then, we have

$$\delta_{win}(r) = w_k \sum_{n=1}^{\infty} b_n r^{2n} \tag{12}$$

For fused silica, $dn/dT \approx 1 \times 10^{-5}\,^{\circ}C^{-1}$, $\alpha = 0.35 \times 10^{-6}\,^{\circ}C^{-1}$[11], $\nu = 0.17$[12], $P' = 0.2$[13]. It is apparent that dn/dT in w_k plays a determining role.

2.3. Effect of composite thermal lens

In an electrically discharged gas and the window opening, when the focal length of the thermal lens is considerably greater than the device length, it is convenient to use the light focal power to describe the state of the equivalent optical system. Assume F is the overall thermal-lens focal length, and is the overall aberration, then

$$\frac{1}{F} = 2\frac{\delta_{tot}(r)}{r^2} \tag{13}$$

$$\delta_{tot}(r) = \delta_{gas}(r) + 2\delta_{win}(r) \tag{14}$$

From Eqs. 6, 12, 13 and 14, the light focal power of the overall thermal lens is

$$\frac{1}{F} = -\frac{lC_{equ}pP}{2\lambda_0 kT^{m+1}(0)} \times \frac{1}{T(r)} + 4w_k\left(b_1 + \sum_{n=1}^{\infty} b_{n+1}r^{2n}\right) \tag{15}$$

The relation between thermal lens and the inputted electric power is relatively complex. When the temperature field remains unchanged, the light focal power is proportional to the atmospheric pressure. In the expression for the light focal power of the thermal lens at the window, term b_1 shows that the focal length of thermal lens is not related to r when the temperature field is parabolically distributed. Terms b_2, b_3 and so on reveal the non-binomial property of the thermal lens. In other words, the focal length of thermal lens is not uniform in the diametral direction.

III. Measurement of Thermal Lens

Fig. 1(a) shows a measurement set-up when measuring a

thermal lens with the light-beam deflection method. After the He-Ne laser beam passes through a small aperture of a telescope with beam expansion and collimation, the beam is illuminated onto a light shield with three small holes (each 4.5mm in diameter). Beyond the light shield, the three beams are arranged on a straight line; the central light beam passes through the center of the electrical discharge tube; the two other beams maintain their distances from the axis center, r_1 and r_2, respectively. A spectroscope is used to eliminate interference of superradiation by the copper-vapor laser. Beyond a reflective mirror and a light filter, three light beams are incident onto an array plane of photoelectric diodes. Fig. 1(a) shows the spatial relation between the diode array plane and light beam. The diffraction fringe of the light beam on the array plane is the Fraunhofer diffraction of circular holes. From a model 4400 Boxcar, specimens are collected for the light intensity distribution at AB in the figure. The specimens are averaged ten times in order to reduce the effect of electrical discharge perturbations. The intensity center of the Airy spot is taken as the light beam center. From the centers of the three light beams, r_1 and r_2 as well as the deflection quantities Δ_1, Δ_2 (after the thermal lens is traversed by the light beam) can be determined.

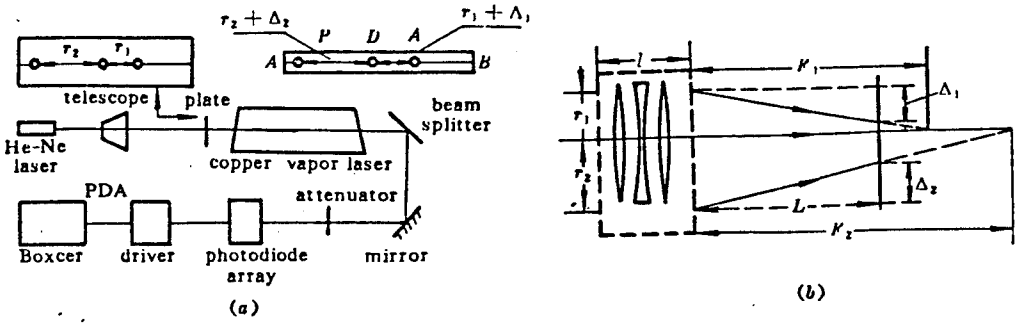

Fig. 1

(*a*) Schematic diagram of the appratus for measuring the thermal lens of the copper vapor laser;

(*b*) Schematic diagram for calculating focal lengthes

Fig. 1(b) is a block diagram for calculating the focal length of the thermal lens. In the experiment, the length (of

copper-vapor laser device) $l = 1.5\,\mathrm{m}$; the inner diameter (of the electrical discharge electrode) 2R=35mm; the spacing (of the electrodes) is 890mm; the diameter (of the fused silica window) D=70mm and thickness d=6mm. From copper-vapor laser device to the photoelectric diode array plane, the distance L=21m; r_1=6.20mm and r_2=9.13 mm. For a thermal lens of hundred-meter magnitude, the laser device can be considered as an equivalent thin lens. From the geometric relationship in Fig. 1, the thermal-lens focal length (at different radii) is

$$F_i = L(r_i/\Delta_i) \quad (i = 1,2) \tag{16}$$

In the measurement method mentioned above, the error is primarily caused by error in positioning the central point of the light beam; the error of the light focal power is $\pm 1\times 10^{-3}\,\mathrm{m}^{-1}$.

In Fig. 2(a), an interference method is used to observe and measure the thermal-lens effect at the window opening. In the figure, BS is a spectroscope (one side of which is antireflective; and the other side is semi-transparency and semi-reflective). In Fig. 2(b), after the collimated parallel light rays are reflected from two surfaces before and after the window opening, an interference fringe is formed on the reception plane. In an actual case, the window opening has a certain wedge angle; its magnitude can be obtained from the parallel interference fringe when power is not applied. During electrical discharge, the thermal lens at the window opening is primarily determined by dn/dT. The deformation of window opening is very small; therefore, it can be assumed that the front and rear surfaces of the window are maintained as planes. The interference fringe is the result of interference between the plane wave (reflected from the front surface of the window) and the slightly inclined converging spherical-surface wave (reflected from the rear surface of the window). The convergent wave is formed with two passages through the window opening by the plane wave acting as a thermal lens. Hence, causing this convergent spherical-surface

wave, the thermal-lens focal length F'_{min} is a composite focal length corresponding to a thermal lens of two layers of window. Aberrations at various points in the interference field are superimposed by aberrations caused by slant wedge and thermal lens. In making an analysis of this type of interference, please refer to reference [14]. In Fig. 6(b), the geometric relation between the geometric center of the window opening, and the eccentric interference ring center can rely on the following equation to calculate the focal length F'_{min} of the equivalent thermal lens.

$$F'_{min} = r_k^2/2K\lambda \tag{17}$$

λ is wavelength of the He-Ne laser; r_k is the length AD in the figure.

For long focal lengths, under thin-lens approximation conditions, F'_{min} is equal to the composite focal length of the thermal lens at the bilayer window of the laser device. No further explanation will be made in the discussion that follows.

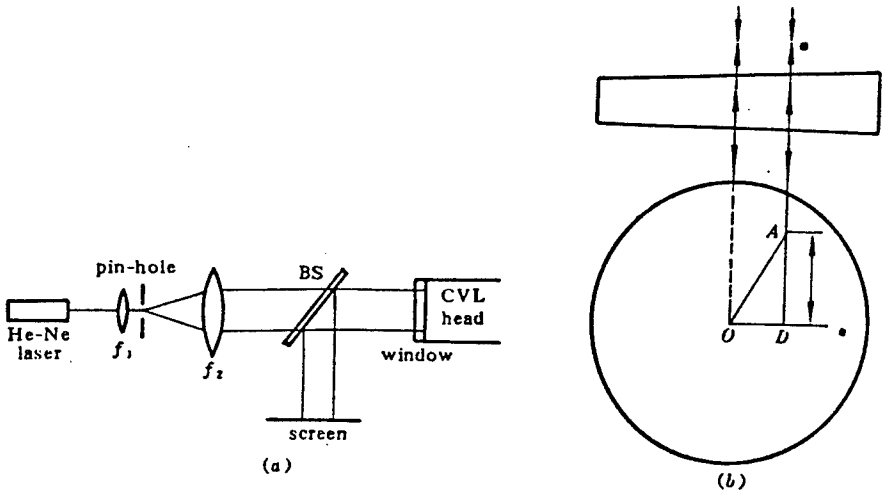

Fig. 2

(a) Schematic diagram of the interferometer for measuring the thermal lens of the fused silica windows; (b) Schematic of the interferogram

IV. Experimental Results and Discussion

Fig. 3 shows the dynamic variation process of a thermal lens at different input electrical power at the same gas pressure. When the power is just barely applied, an instantaneous negative lens is formed in the electrical discharge tube. The size of the negative lens is related to the input power and the initial conditions in the electrical discharge tube. With increasing electrical discharge time, the gas negative lens and the positive lens (at the window opening) gradually reach equilibrium with thermal equilibrium being attained. To verify the gas lens characteristics, the right side of the dashed lines in Fig. 3 shows the variation state of the thermal lens after electrical discharge is stopped. Since the thermal lens at the window opening can change rapidly (this can be verified in the interference diagram), and since the temperature gradient within the electrical discharge tube weakens rapidly, thus from the intensifying of positive-lens effect in the figure, it can be expected that while in operation the gas exhibits a negative-lens effect.

Refer to Fig. 4 for the thermal-lens effect of the device when heat equilibrium is reached. With increasing electric power inputted, the positive-lens effect at the window opening is also intensified. The gas negative lens is determined by Eq. 6. The overall thermal-lens effect changes from negative to positive; moreover, values are different at different radii. When the input electric power is low, the gas negative-lens plays a major role; conversely, the positive lens at the window opening plays a major role.

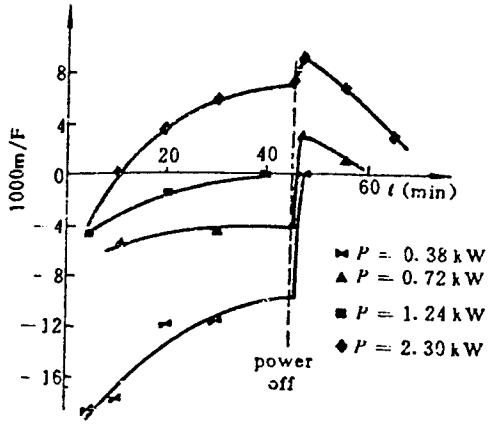

Fig. 3 The temporal evolution of the thermal lens at different input powers at measuring point r_2; $p =$ 10 Pa

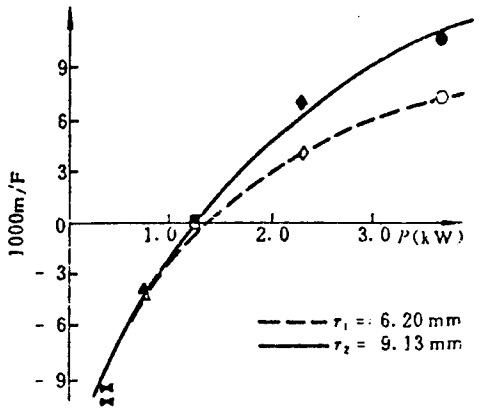

Fig. 4 Dependences of the thermal lens on input power at two measuring points r_1, r_2; $p = 10$ Pa

When the input electric power is the same but the gas pressure is different, since the heat conductivity of gas is only related to temperature, $\lambda = \lambda_0 T^m$ [8], if the power distribution and the boundary conditions remain unchanged, the temperature-field distribution can be considered as unchanged. When the positive lens at the window opening remains unchanged, the effect of the negative gas lens intensifies as the gas pressure is increased. The variation of overall thermal-lens effect can be observed from Fig. 5.

Fig. 6 shows typical variations of interference fringes caused by the window-opening thermal lens. Fig. 6(a) shows an interference diagram when power is not applied. The slant wedge of the window forms straight stripes fundamentally parallel among them. With increasing input power, deformation at the window opening gradually becomes more and more serious, see Fig. 6(b) and (c). In the direction parallel to the original stripes,

Eq. 17 can be applied to estimate the focal length of the thermal lens.

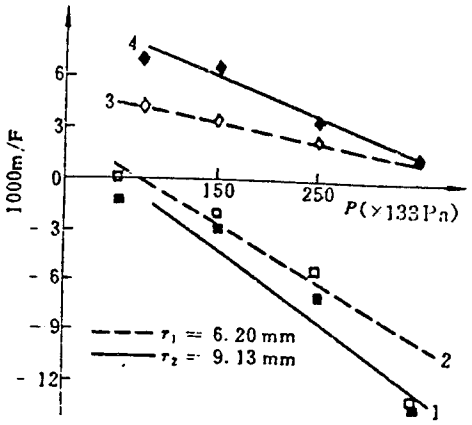

Fig. 5 Dependences of the thermal lens on gas pressure at two measuring points r_1, r_2 when input powers are 1.24 kW (1,2) and 2.3 kW (3,4)

Fig. 6 Typical interferograms of one window for input power of 0 (*a*), 1.24 (*b*), and 3.76 kW (*c*); p = 10 kPa

Finally, the authors visualize the situation of P=3.76kW and p=10kPa. Here, the focal length of thermal lens at the window opening can be calculated from Fig. 6(c); when K=4, r_1=19.5mm; then F'_{min}=75m. In Eq. 6, we can refer to reference [12] and with conversion, C_{equ} is approximately $2.6\times10^{-30}m^{-3}$. Assume T_w=1500°C, then the center temperature is 3232°C. At r_2, the gas thermal lens is -400m. Composed of two thermal lenses, it will be a 92m

positive lens. This is consistent with the experimental result in Fig. 4.

The authors express their gratitude to professor Yao Zhixin of Zhejiang University for his beneficial discussion, and to instructors Xu Yuguang and Xu Deyan for their advice in making measurements.

The first draft of the paper was received on 4 June 1993; the final, revised draft was received for publication on 13 August 1993.

REFERENCES

1 V. M. Zharikov, V. V. Zubov *et al.*. *Sov. J. Quant. Elect.*, 1984, **14(5)**: 623
2 S. K. Dixit, B. Singh *et al.*. *Opt. Lett.*, 1990, **15(8)**: 429
3 R. Bhatnagar, S. K. Dixit *et al.*. *Opt. Commun.*, 1989, **74(1,2)**: 93
4 R. Bhatnagar, S. K. Dixit *et al.*. *Opt. Commun.*, 1991, **82(5,6)**: 557
5 S. K. Dixit, J. K. Mittal *et al.*. *Opt. Commun.*, 1992, **88(4,5,6)**: 397
6 M. Amit, S. Lavi *et al.*. *Opt. Commun.*, 1987, **62(2)**: 110
7. Shen Qimin and Liang Peihui, GUANGXUE XUEBAO [JOURNAL OF OPTICS], 1987, 7(2), page 112.
8 M. J. Kusher, B. E. Warner. *J. Appl. Phys.*, 1983, **54(6)**: 2970
9 L. B. Direktor, M. M. Malikov *et al.*. *High Temperature*, 1983, **21(1)**: 146
10 William, A. Molander. *SPIE*, 1989, **1041**: 11
11. Li Jingzhen (chief editor), GUANGXUE SHOUCE [HANDBOOK ON OPTICS], Shenxi: Shenxi Publishing House, 1985, pages 1292 and 1337.
12. Fantian Xiuyi et al, WULIXUE CHANGYONGSHUBIAO [TABLES ON FREQUENTLY USED NUMBERS IN PHYSICS], Beijing: Science Publishing House, 1987, pages 25 and 162.
13 R. W. Dixon. *J. Appl. Phys.*, 1967, **38**: 5149
14. Chen Zousheng and Gao Yingjun, GUANGXUE XUEBAO, 1984, 4(7), page 593.
15 C. A. Klein, *Opt. Eng.*, 1990, **29(4)**: 343

DISTRIBUTION LIST

DISTRIBUTION DIRECT TO RECIPIENT

ORGANIZATION	MICROFICHE
B085 DIA/RTS-2FI	1
C509 BALL0C509 BALLISTIC RES LAB	1
C510 R&T LABS/AVEADCOM	1
C513 ARRADCOM	1
C535 AVRADCOM/TSARCOM	1
C539 TRASANA	1
Q592 FSTC	4
Q619 MSIC REDSTONE	1
Q008 NTIC	1
Q043 AFMIC-IS	1
E051 HQ USAF/INET	1
E404 AEDC/DOF	1
E408 AFWL	1
E410 AFDIC/IN	1
E429 SD/IND	1
P005 DOE/ISA/DDI	1
P050 CIA/OCR/ADD/SD	2
1051 AFIT/LDE	1
P090 NSA/CDB	1
2206 FSL	1

Microfiche Nbr: FTD94C000564
NAIC-ID(RS)T-0704-94